In situ oxidation of sulfide minerals supports widespread sulfate reducing bacteria in the deep subsurface of the Witwatersrand Basin (South Africa): insights from multiple sulfur and oxygen isotopes

Long Li[a,*], Siwen Wei[a], Barbara Sherwood Lollar[b], Boswell Wing[c,d], Thi H. Bui[d], Shuhei Ono[e], Maggie C. Y. Lau Vetter[f,g], Tullis C. Onstott[g], Thomas L. Kieft[h], Gaetan Borgonie[i], Borja Linage-Alvarez[j], Olukayode Kuloyo[j,1], Esta van Heerden[j]

[a] Department of Earth and Atmospheric Science, University of Alberta, Edmonton, AB, Canada

[b] Department of Earth Sciences, University of Toronto, Toronto, ON, Canada

[c] Geological Sciences, University of Colorado Boulder, Boulder, Colorado, USA

[d] Department of Earth and Planetary Sciences and GEOTOP, McGill University, Montreal, Quebec, Canada

[e] Department of Earth, Atmospheric, and Planetary Sciences, Massachusetts Institute of Technology, Cambridge, MA, USA

[f] Institute of Deep-sea Science and Engineering, Chinese Academy of Sciences, Sanya, Hainan, China

[g] Department of Geosciences, Princeton University, Princeton, NJ, USA

[h] Department of Biology, New Mexico Institute of Mining and Technology, Socorro, NM, USA;

[i] Extreme Life Isyensya, Gentbrugge, Belgium

[j] Department of Microbial, Biochemical, and Food Biotechnology, University of the Free State, Bloemfontein, South Africa

[1] Present address: Shell International Exploration and Production Inc, Westhollow Technology Center, Houston, TX, USA.

* Corresponding author. E-mail address: long4@ualberta.ca (L. Li)

Keywords:

Subsurface biosphere; Witwatersrand Basin; sulfide oxidation; microbial sulfate reduction; multiple sulfur isotopes; oxygen isotopes.

Abstract

Dissolved sulfate is a crucial electron acceptor for the subsurface biosphere, particularly for the living microbial ecosystems in the long-isolated (on the order of millions to billions of years) deep subsurface fracture waters in Precambrian cratons, e.g., in the Witwatersrand Basin of the Kaapvaal Craton, South Africa. Aiming to understand the role of sulfate in the sustainability of the subsurface habitat and the spatial extent of the terrestrial subsurface biosphere, we carried out a basin-scale examination on the source and producing mechanisms of dissolved sulfur (sulfate and sulfide) in the subsurface fracture waters in the Witwatersrand Basin using multiple sulfur isotopes ($^{32, 33, 34, 36}S$) and oxygen isotopes ($^{16, 18}O$). Dissolved sulfate in 14 fracture water samples collected from 900 to 3,413 meters below the surface at 6 sites show isotopic ranges from –5.3‰ to +19.4‰ for $\delta^{34}S$, –0.40‰ to +0.50‰ for $\Delta^{33}S$, and –1.1‰ to +10.9‰ for $\delta^{18}O$. These isotopic signature are distinct to those of the sulfate minerals (e.g., the carbonate-associated sulfate in local Transvaal Supergroup dolomite sequences: $\delta^{34}S$ = +31.4‰ to +39.2‰; $\Delta^{33}S$ = –0.01‰ to +0.16‰), but identical to those of the sulfide minerals in the host rocks. This indicates that the dissolved sulfate in the fracture waters were dominantly generated by in situ oxidation of sulfide minerals at basin scale, although mixing of a small amount of surface sulfate at some sites cannot be completely ruled out. The dissolved sulfate in the less deep and less saline fracture waters are in oxygen isotope disequilibrium with their host waters, a surprising result given that the water residence times are orders of magnitude longer than the

time required for oxygen isotope exchange to reach equilibrium. This implies that vigorous in situ sulfate production has occurred after the fracture waters were isolated. In contrast, the dissolved sulfate in the deeper, more saline waters are in apparent oxygen isotope equilibration or close to equilibration with their host waters. This might be attributed to a combined effect of faster oxygen isotope exchange with water at higher temperatures, larger extent of sulfate reduction, and/or less efficient sulfate production. The dissolved sulfide in the fracture waters has similar $\Delta^{33}S$ values but is 3.0‰ to 26.4‰ lower in $\delta^{34}S$ than coexisting sulfate, suggesting that the dissolved sulfide is mostly generated from bacterial sulfate reduction, which is consistent with the widespread existence of sulfate-reducing bacteria down to >3.4 km below surface in the Witwatersrand Basin. Overall, these novel isotopic results demonstrate that geological processes can provide a steady long-term sulfate source in deep fracture fluids by in situ oxidation of sulfide minerals in their host rocks, and thereby a mechanism to sustain the terrestrial subsurface biosphere, even in deep, high-temperature, long-isolated water systems. Thus, sulfate as a terminal electron acceptor is not the limiting factor for the spatial expansion of terrestrial subsurface biosphere.

1. Introduction

The Witwatersrand Basin in the Kaapvaal craton, South Africa contains gold- and uranium-bearing reefs (Fig. 1) deposited between < 2,985 and > 2,714 Ma (Guy et al., 2012). Mining within these rock layers has encountered abundant fracture fluids with variable geochemical signatures and diverse microbial ecosystems at levels as deep as 3.9 kilometers

below the surface (kmbls) (e.g., Moser et al., 2003; Lin et al., 2006; Onstott et al., 2006; Lau et al., 2016; Magnabosco et al., 2018).

Previous studies have shown that these fracture waters contain noble gas components of > 2 billion years in age (Lippman-Pipke et al., 2011), in some cases mixing with modern and paleo-meteoric water (Borgonie et al., 2015). Their geochemical and isotopic signatures have been largely overprinted by fluid-rock interaction (e.g., Ward et al., 2004; Onstott et al., 2006; Sherwood Lollar et al., 2006; Heard et al., 2018; War te al., 2021). Shallow fracture waters (e.g., < 1 kmbls) have relatively low temperature and salinity with large proportion of meteoric water, and contain dissolved gases dominated by CH_4 and N_2 with variable but generally small amounts of O_2. In contrast, deep fracture waters (particularly those >2.5 kmbls) tend to have relatively high temperatures (up to > 60 ºC) and salinities, and contain dissolved gases dominated by C_{1-4} alkanes, N_2, He and H_2 (Lippmann et al., 2003; Ward et al., 2004; Onstott et al., 2006; Silver et al., 2012), though with notable exceptions at the Tau Tona (Magnabosco et al., 2015) and Kopanang (Borgonie et al., 2015) gold mines where low salinity paleometeoric waters are also found at great depth. Noble gas and ^{36}Cl measurements of the fracture waters from 0.7 to 3.3 kmbls in the Carletonville (e.g., the Kloof, Tau Tona, Driefontein and Mponeng mines), Welkom (e.g., the Beatrix, Masimong mines), and Evander goldfields in the Witwatersrand Basin revealed that the water residence times generally increased from as low as hundreds of thousand years in the shallow waters to as high as 170 million years in the deep saline waters (Lippmann et al., 2003; Lippmann-Pipke et al., 2011; Heard et al., 2018).

Microbial abundance and diversity also vary significantly at different locations and depths. Taxonomic diversity of the fracture waters varies from several hundred bacterial genera (Magnabosco et al., 2014) to one (Lin et al., 2006b; Chivian et al., 2008). The micobes are

dominated by Proteobactia and Firmicutes. Archaea, mainly Euryarchaeota, are almost always present but in far lesser abundance and diversity than bacteria (Lau et al., 2014; Takai et al., 2001; Moser et al., 2005). Eukarya, most notably members of Nematoda, are present in lesser abundance in the shallower fracture water (Borgonie et al., 2015). Viruses also comprise a significant fraction of the biomass (Labonté et al., 2015). Microbial taxonomic and functional composition does not correlate with depth or the geochemical parameters (Magnabosco et al., 2014; Lau et al., 2014).

Despite the large variations in microbial biomass and biodiversity, molecular investigations have unambiguously shown that sulfate-reducing bacteria are widespread in the subsurface fracture waters in the Witwatersrand Basin and even become the dominant species in the deep saline fracture water at one site (i.e., Mponeng; Lin et al., 2006; Chivian et al., 2008). Sulfate-reducing bacteria are also important constituents of deep subsurface fracture waters in the Canadian Shield (Onstott et al., 2009; Lollar et al., 2019) and the Fennoscandian Shield (Hallbeck and Pedersen, 2008; Pedersen et al., 2014; Purkamo et al., 2017). In order to understand the ecological structure and the spatial extent of the deep biosphere in Precambrian cratons, it is therefore crucial to understand the origin and sustainability of sulfate in subsurface fracture waters.

Several possible processes could possibly supply sulfate to the subsurface fracture waters in Precambrian cratons including the Witwatersrand Basin: (1) infiltration of surface sulfate; (2) leaching of sulfate minerals (if there are any) or carbonate-associated sulfate (CAS) in host rocks; and (3) in situ oxidation of sulfide minerals in host rocks, e.g., by oxidants from water radiolysis (Vovk, 1987; Lin et al., 2006; Lefticariu et al., 2010; Li et al., 2016).

Multiple sulfur isotopes have been demonstrated to be a robust tool to trace sulfur sources and sulfur recycling processes (e.g., sulfide oxidation and sulfate reduction) in fracture waters in Precambrian cratons (Lin et al., 2006; Li et al., 2016). This is attributed to two major features of the sulfur isotope system. First, the sulfur mass dependent fractionations (S-MDF) associated with sulfide oxidation and sulfate reduction are very different. With few exceptions (Pellerin et al., 2019), oxidation of sulfide minerals (either biologically or abiotically) generally has very minor isotope discrimination and thus the sulfate product shows similar or slightly lower $\delta^{34}S$ value than precursor sulfide (Seal, 2006). In contrast, bacterial sulfate reduction (BSR) shows variably larger isotope fractionation (e.g., Sim et al., 2011 and references therein), resulting in significantly lower $\delta^{34}S$ values in the sulfide product than precursor sulfate. Second, sulfide and sulfate minerals in the Archean supracrustal rocks often bear unique sulfur mass independent fractionation (S-MIF) signals (Farquhar et al., 2000). The magnitudes of S-MIF signals, which can be expressed by

$$\Delta^{33}S = \delta^{33}S - 1000 \times [(1 + \delta^{34}S/1000)^{0.515} - 1] \quad (1)$$

display a large range from < –2‰ to > +12‰ in the Archean, but quickly diminish to a small range of 0‰ to +1‰ during the period between 2.0-2.4 Ga, and remain at near 0‰ after 2.0 Ga (Farquhar et al., 2000; Ono et al., 2003). Accordingly, S-MIF signals can be used as a diagnostic tracer for probing the sulfur recycled from sulfide and sulfate minerals before at least 2.0 Ga, and possibly 2.45 Ga, depending on the magnitude of S-MIF signals (e.g., Li et al., 2016). Based on multiple sulfur isotopic comparison between dissolved sulfate and sulfide in a ~20 million-year-old, high-temperature, saline fracture water system and associated barite and pyrite fracture minerals at 2.8 kmbls of the Mponeng gold mine, Lin et al. (2006) deduced an origin of the dissolved sulfate with 30% from in situ pyrite oxidation and 70% from hydrothermal barite

dissolution. A similar study in the Canadian Shield shows that the dissolved sulfate in the billion-year-old fracture water from the Kidd Creek mine is nearly all formed by in situ oxidation of sulfide minerals (Li et al., 2016).

Oxygen isotopes of sulfate ($\delta^{18}O_{sulfate}$) can provide additional insights into the sources and processes involved in the sulfur cycle in the subsurface fracture waters. For example, the $\delta^{18}O$ value of sulfate produced by sulfide oxidation is strongly dependent on the $\delta^{18}O$ values of H_2O and O_2. Secondary processes, e.g., SO_4^{2-}–H_2O isotope exchange and BSR, may further overprint the $\delta^{18}O_{sulfate}$ values. Modeling of $\delta^{18}O_{sulfate}$ values may thus provide constraints on the extent and time scales of these reactions.

In this study, we examined the $\delta^{34}S$ and $\Delta^{33}S$ values of coexisting dissolved sulfate and sulfide, as well as the $\delta^{18}O$ values of dissolved sulfate and host fracture waters, for 14 samples from 6 sites in the Witwatersrand Basin. For comparison, we also measured the $\delta^{34}S$, $\Delta^{33}S$ and $\delta^{18}O$ values of CAS in the Transvaal dolomite that hosts the paleo-meteoric endmember for some of the fracture waters. These data are integrated to unravel the source, formation mechanism and microbial utilization of dissolved sulfate in the deep subsurface fracture waters in the Witwatersrand Basin, which has important implications for Precambrian continental systems worldwide, and similar environments on other rocky planets (e.g., Mars) and moons.

2. Material and methods

2.1. Geological background and sampling sites

The rock sequences in the studied area consist of, from bottom to top, the Witwatersrand Supergroup, Ventersdorp Supergroup, Transvaal Supergroup and Karoo Supergroup (Fig. 1).

These sedimentary sequences unconformably overlie the > 3.09 Ga granite-greenstone basement (Robb and Meyer, 1995). The fracture water samples mainly came from the Witwatersrand Supergroup, Ventersdorp Supergroup, and Transvaal Supergroup (Fig. 1; Appendix Table A.1). The Witwatersrand Supergroup was formed from ~3.0 Ga to 2.8 Ga and can be divided into two subdivisions – the West Rand Group (WRG) and the Central Rand group (CRG). The WRG was formed in shallow marine or intertidal environments, and is mainly composed of shales, sandstones, argillites, greywacke, and minor quartzite (Frimmel, 2005). The CRG represents braided stream deposits dominated by conglomerates and fluvial sands with minor shales (Coward et al., 1995; Robb and Meyer, 1995; Frimmel, 2005). The ~2.7 Ga Ventersdorp Supergroup unconformably overlying the Witwatersrand Supergroup is mainly composed of flood basalts (Coward et al., 1995; Frimmel, 2005). The Transvaal Supergroup was deposited in ~2.5 Ga in a shallow marine environment (Martin et al., 1998; Frimmel, 2005) and mainly composed of dolomite with banded iron formations and volcanics. The Witwatersrand Basin experienced a significant meteorite impact at ~2.025 Ga, namely the Vredefort event (Coward et al., 1995). No younger geological formations are preserved in the region except some young (254 to 190 Ma) fluvial sedimentary rocks and flood basalts, i.e., the Karoo Supergroup, which only appears on the southern and eastern parts of the Witwatersrand Basin (Johnson, 1996). Sedimentary sulfate deposits are absent from all of these geological strata and minor hydrothermal barite has been observed in the quartz veins in the Ventersdorp Contact Reef (Johnson et al., 1996; Gartz and Frimmel, 1999; Frimmel, 2005).

Fracture water samples were collected from 0.9 to 3.4 kmbls in 4 mines (Kloof, Tau Tona, Driefontein and Mponeng) in the Carletonville region, and from 1.3 to 1.9 kmbls in 2 mines (Joel and Masimong) in the Welkom region of the Witwatersrand Basin (Fig. 1; Table

A.1). The genetic potential for BSR has been reported for some of the same boreholes, e.g., Tau Tona (Magnabosco et al. 2015), Driefontein (Gihring et al. 2006), Mponeng (Becraft et al. 2021). Recent noble gas studies (Heard et al., 2018) on some of the samples studied here yielded conservative estimates of water residence times of 40-97 Ma (mean 85 Ma; closed system) or 3.4-10.8 Ma (open system) for MM546, 2.6-12.0 Ma (closed system) or 0.2-0.69 Ma (open system) for DR5IPC, and 0.77-6.1 Ma (mean 5.9 Ma; closed system) or 0.1-1.0 Ma (open system) for TT107 (Table A.2). Noble gas modeling (Heard et al., 2018) and ^{14}C investigations (Simkus et al., 2016) suggested that TT107 samples represented a mixture between 2.0 Ga hydrothermal fluid and fresh, 1-6 kyr old meteoric water which infiltrated to 3.0 kmbls along the fractured margins of cross-cutting Karoo dykes (Simkus et al., 2016). The Kloof samples were collected from a borehole intersecting the Danys fault at 3.27 kmbls. Fracture water from this same fault but collected at 3.08 kmbls yielded noble gas-derived residence times of 95-105 Ma (closed system) or 12-16 Ma (open system) (Lippmann et al., 2003). Lin et al. (2006) reported residence times of 15.8-25 Ma for a more saline fracture water from Mponeng collected at a location different from these two sampled boreholes in this study.

The Malmani Dolomite Subgroup of the Transvaal Supergroup is a regional aquifer and intersected by all of the Carletonville mines. Water from the Malmani Dolomite is accessed from the subsurface of the Driefontein mines and used as mining water in the Carletonville region (Onstott et al., 2003). In the north part of Welkom, the Transvaal Supergroup is absent and the Karoo Supergroup lies directly on the Ventersdorp Supergroup. For comparison, 5 dolomite rock specimens were collected from the Transvaal Supergroup in the Driefontein mine for the study of CAS.

2.2. Sample collection, processing and isotope measurements

All equipment was cleaned and sterilized prior to use. Fracture waters were introduced from borehole through a custom-made manifold to sampling device (Lau et al., 2016). Prior to sampling, the manifold and sampling device were flushed by borehole water to minimize potential contamination.

Basic water properties, including temperature, pH, conductivity and/or salinity, and Eh, were measured onsite using portable probes. Dissolved sulphide, oxygen, total and ferrous iron were measured with CHEMets® kits. Aqueous chemistry (anions and cations) and stable isotope composition ($\delta^{18}O$ and $\delta^{2}H$, relative to the Vienna Standard Mean Ocean Water or VSMOW standard) of the fracture waters were analyzed at Princeton University and the University of Waterloo, respectively.

For the study of dissolved sulfate, water was filtered through a 0.2-micron filter and placed into a 1 L high-density polyethylene bottle pre-loaded with ~1 g $CdCl_2$ powder, which can quickly fix dissolved reduced sulfur species (H_2S, HS^- and S^{2-}) as CdS to prevent oxidation of these sulfur species by atmospheric O_2 during sample transportation and storage. In the laboratory, dissolved sulfide in a sample (already precipitated as CdS) was collected first by filtration, after which the dissolved sulfate was precipitated as $BaSO_4$ and collected by filtration following the method described by Li et al. (2016). The CAS in the Malmani dolomite was extracted following the published protocols (e.g., Kampschulte et al., 2001; Edwards et al., 2019). Sulfate from each step of the protocol was precipitated as $BaSO_4$ and collected by filtration.

To ensure the purity of $BaSO_4$ precipitates from both fracture water samples and dolomite samples for isotope analyses, all $BaSO_4$ samples were examined by scanning electron

microscopy (SEM) at University of Alberta. Elemental analysis by the equipped energy dispersive X-ray spectroscopy (EDS) on the SEM verified that all $BaSO_4$ precipitates were pure. No carbonate, nitrate, or hydrosilicic precipitate was detected.

Multiple sulfur isotope compositions of these CdS and $BaSO_4$ precipitates were measured at McGill University and Massachusetts Institute of Technology. Sulfur in $BaSO_4$ or CdS was converted into H_2S, which was then trapped by zinc acetate solution and precipitated as ZnS. The yielded ZnS was further converted to Ag_2S by adding excess $AgNO_3$ solution. The Ag_2S was dried and reacted overnight with F_2 to produce SF_6 gas, which was then purified by a preparatory gas chromatography for multiple sulfur isotope measurements on a Thermo Finnigan MAT 253 mass spectrometer. All sulfur isotope data are reported relative to the Vienna Canyon Diablo Troilite (VCDT) standard (Ono et al., 2012). The analytical uncertainty (2σ) is 0.2‰ for $\delta^{34}S$ and 0.01‰ for $\Delta^{33}S$.

Oxygen isotope compositions of sulfate were measured by a TC/EA-CF-IRMS instrument at University of Calgary. $BaSO_4$ samples were heated to 1450 ˚C in a high-temperature reactor with graphite to produce CO, which was then carried by a helium flow to a Thermo Delta + XL mass spectrometer for oxygen isotope analysis. $\delta^{18}O$ values are reported relative to the VSMOW standard with an analytical uncertainty of 0.2‰ (2σ).

3. Results

The studied fracture waters at 0.9 to 1.0 kmbls in the Malmani Dolomite aquifer (Driefontein) have relatively low temperatures of 24-27 ºC, whereas the others at 1.3 to 3.4 kmbls in the Witwatersrand and Ventersdorp supergroups have relatively high temperatures of

40-65 ºC (Table A.1). The waters are near neutral to slightly alkaline and belong to the Na-Cl type, similar to the subsurface fracture waters from other Precambrian cratons globally (e.g., Kietäväinen et al., 2013; Li et al., 2016). The Driefontein and Tau Tona samples are fresh waters, whereas the Joel, Masimong, and Kloof samples are brackish. The two water samples from Mponeng show more variable salinity, with one fresh water and one saline water.

Dissolved sulfate was detectable in all samples with concentrations varying from 7 µM in MM546 to 1,170 µM in TT118 (Table A.1), which fall in the range of previously reported fracture water data in the Witwatersrand Basin (Onstott et al., 2006). Most of the deep (>3 kmbls) fracture waters have sulfate concentrations around 100 µM, similar to those of the deep saline fracture waters from Kidd Creek in the Canadian Shield (Li et al., 2016). Dissolved sulfide is low (< 10 µM or even below detection limit of 0.01 µM) in all samples except TT109 (194 µM).

The $\delta^{34}S$ values of dissolved sulfate vary from –5.3‰ to +19.4‰, which are 3.0-26.4‰ higher than those of coexisting sulfide (Table 1). The $\Delta^{33}S$ of dissolved sulfate vary from –0.40‰ to +0.50‰, which are either identical to or slightly lower (for up to 0.18%) than those of coexisting dissolved sulfide. In contrast, the CAS of the Malmani dolomites show much higher $\delta^{34}S$ values (+31.4‰ to +39.2‰) and more narrow $\Delta^{33}S$ range (–0.01‰ to +0.16‰) (Table 2). The $\delta^{18}O$ of the dissolved sulfate vary from –1.1‰ to +10.9‰, which are 5.4-18.5‰ higher than their host waters (Table 1).

4. Discussion

4.1. Characterization of fracture waters

The $\delta^{18}O$ and $\delta^{2}H$ values of fracture water samples from Tau Tona, Driefontein, Joel, and Masimong (Table 1) all lie on or close to the Global Meteoric Water Line (GMWL) or the Local Meteoric Water Line (LMWL), but are more depleted in ^{18}O and ^{2}H than the mean value of modern annual precipitation from the closest station in Pretoria, South Africa (Fig. 2). This isotopic depletion is consistent with previous studies showing that the fracture waters in the Witwatersrand Basin contain significant components of paleo-meteoric water (Lippmann et al., 2003; Ward et al., 2004; Onstott et al., 2006; Heard et al., 2018). In contrast, the Kloof samples diverge from the LMWL and GMWL toward an endmember close to that defined by the billion-year-old fracture waters of the Canadian Shield sampled at the Kidd Creek Observatory in Timmins, Ontario. This is a typical feature for saline waters and brines in Precambrian cratons attributed to long-term water-rock isotope exchange (Lippmann et al., 2003; Ward et al., 2004; Onstott et al., 2006; Li et al., 2016; Warr et al., 2021). The Mponeng samples in this study were not measured for $\delta^{18}O$ and $\delta^{2}H$, but previous studies (Lin et al., 2006; Onstott et al., 2006) showed that Mponeng waters were also on or above the LMWL (Fig. 2).

4.2. Sulfur source of the dissolved sulfate in subsurface fracture waters

Dissolved sulfate in the studied samples show non-zero $\Delta^{33}S$ with both negative and positive values. The overall $\Delta^{33}S$ range of the dissolved sulfate (from –0.40‰ in MP99 to +0.50‰ in DR9IPC; Fig. 3) is 90 times greater than the analytical error and 4-5 times larger than the $\Delta^{33}S$ range of the Kidd Creek fracture fluids (Li et al., 2016). These signatures cannot be explained by the small $\Delta^{33}S$ values produced by BSR (Johnston et al., 2007), thermal sulfate reduction (Watanabe et al., 2009), or mixing (Ono et al., 2003). Instead, a more straightforward explanation for these large S-MIF signals is an inheritance from minerals in the >2.0 Ga host rocks.

While both sulfide and sulfate minerals may bear S-MIF signals, sulfate minerals can be excluded from the major source of the dissolved sulfate in the studied samples, for several reasons. First, Archean evaporitic barite/gypsum beddings have not been reported from the study area. Second, although Lin et al. (2006) observed barite in the fracture minerals in the Mponeng gold mine, the barite is characterized by a $\delta^{34}S$ value of 10.1‰ and a negligible S-MIF signal ($\Delta^{33}S$ = 0.02‰), which is in contrast to the large S-MIF signature observed in our studied samples. Third, although the Malmani dolomites contain CAS, their sulfur isotopic compositions ($\delta^{34}S$ = +31.4‰ to +39.2‰; $\Delta^{33}S$ = –0.01‰ to +0.16‰; Table 2) are very different to the fracture waters from Driefontein ($\delta^{34}S$ = –5.3‰ to +1.5‰; $\Delta^{33}S$ = +0.47‰ to +0.50‰; Fig. 3, Table 2), indicating the CAS has little contribution to the dissolved sulfate in the aquifer in the Transvaal Supergroup, and thus little contribution to the fracture waters in the underlying Witwatersrand and Ventersdorp supergroups in the Carletonville area. Furthermore, Onstott et al. (2006) showed that, with increasing salinity and diminishing paleo-meteoric water content in the fracture waters in the Witwatersrand and Ventersdorp supergroups, the sulfate concentration actually increased. This implies a sulfate source within these supergroups. It is worth noting that the relatively high $\delta^{34}S$ values of some dissolved sulfate (e.g., the Mponeng and Kloof samples) are more likely a result of BSR (see Section 4.5) rather than significant contribution of CAS.

Consequently, sulfide minerals in host rocks are considered to be the major source of the dissolved sulfate in the subsurface fracture waters in the Witwatersrand Basin. Previous studies reported $\Delta^{33}S$ values of –2‰ to +2‰ for sulfide minerals in the Witwatersrand Basin (Hofmann et al., 2009; Guy et al., 2012, 2014). Isotopic comparison between the dissolved sulfate in fracture waters and sulfide minerals in host rocks shows that the $\delta^{34}S$ and $\Delta^{33}S$ values of the dissolved sulfate can be well accounted for by the Archean sulfide minerals in the Witwatersrand

Basin (see Fig. 4). In detail, several factors may play a role in controlling the variable $\Delta^{33}S$ signature at different sites. The dissolved sulfate samples have a much smaller $\Delta^{33}S$ range than that of sulfide minerals in host rocks (Hofmann et al., 2009; Guy et al., 2012, 2014; Fig. 4), which may be attributed to a mixing effect of contributing sulfides with heterogeneous $\Delta^{33}S$ values. The $\Delta^{33}S$ values of dissolved sulfate also vary significant from site to site. This may be due to the spatial variability in the $\Delta^{33}S$ of sulfide minerals (Hofmann et al., 2009; Guy et al., 2012, 2014). Even in the same mine (e.g., Tau Tona and Mponeng), dissolved sulfate from different locations can have very different $\Delta^{33}S$ values (Table 1; Fig. 3). This reflects strong control of local fracture networks and hydrological compartment, which could have sampled isotopically heterogeneous sulfide minerals at a small spatial (e.g., meters) scale. It is also noted that the dissolved sulfate in Driefontein show higher $\Delta^{33}S$ values (+0.47‰ to +0.50‰) than those of the pyrites in the underlying Black Carbon Reef (–1.35‰ to +0.18‰; Hofmann et al., 2009), ruling out Black Carbon Reef as the source of dissolved sulfate in the Driefontein samples. In fact, detrital pyrites have been reported to occur widely in the Transvaal Supergroup (e.g., Johnson et al., 2014). We also observed detrital pyrites in the Malmani dolomite host-rock samples. Sulfate formed by reacting the dolomite powder samples with 30% H_2O_2 for 48 hour gave $\Delta^{33}S$ value of +2.65‰ to +4.22‰ (Table 2), indicating that the detrital sulfide in the Malmani dolomite bear highly positive S-MIF signals, which can easily satisfy the observed $\Delta^{33}S$ values of dissolved sulfate.

It is worth noting that ^{14}C analysis identified some more recent (within the last ~20 kyr or so) surface meteoric water recharge into the fracture systems of TT107, TT109 and DR5IPC (Simkus et al., 2016). In these cases, mixing of surface sulfate is possible. However, the $\Delta^{33}S$ values of dissolved sulfate (+0.34‰ to +0.48‰) in these three fracture water systems are among

the highest values in the Witwatersrand basin (Table 1), implying the relative contributions of recent surface sulfate (if there is any) in these fracture waters are insignificant.

4.3. Sulfide oxidation mechanism

The common sulfide oxidation mechanisms include: (1) oxidative weathering, which generally occurs in an environment with free O_2; (2) anaerobic sulfide oxidation, which generally occurs in an O_2-free environment by using Fe^{3+} as oxidant; and (3) oxidation of sulfide by oxidants (e.g., oxygen radicals) from water radiolysis induced by energy released from radiogenic decay of U, Th and K in host rocks (Lin et al., 2006; Lefticariu et al., 2010; Li et al., 2016), a process that has been termed as indirect radiolytic oxidation of sulfide (most commonly pyrite), or IROP (Li et al., 2016). The IROP is a slow abiotic process with low sulfate productivity (Li et al., 2016), whereas oxidative weathering and anaerobic sulfide oxidation may occur either abiotically or biologically in much faster rates.

Although the redox condition and Fe^{3+} concentrations have been measured for each fracture water system (Table A.1), the sulfate productivities from oxidative weathering and anaerobic sulfide oxidation are difficult to quantify due to the lack of constraints on sulfate production rates in corresponding environment. In contrast, the sulfate productivity from IROP can be modeled by the method described in Li et al. (2016) for reference. Using the U, Th, K concentrations and rock porosities summarized by Lin et al. (2005a, b) and the sulfur concentration of 0.02% to 1.3% (Guy, 2012) for the host rocks in the Witwatersrand Basin, a ballpark estimation on the sulfate productivity by IROP for various lithologies and the accumulated sulfate concentrations in the fracture waters over time are listed in Table A.3 and A.4. Due to the large variation in U, Th, K and sulfide concentrations, the modeling results have large uncertainties. Nevertheless, the modeling results indicate that, without taking the BSR

effect into account, the sulfate produced solely by IROP over the residence times of the studied fracture waters can bracket the observed values in Kloof and Masimong, but are slightly lower than the observed concentrations in Mponeng and Tau Tona and orders in magnitude lower than the observed concentrations in Driefontein (Table A.4). This ballpark estimation is in general agreement with the redox conditions of these fracture systems. For example, the Driefontein waters are relatively oxic (Table A. 1; Onstott et al., 2006; Simkus et al., 2016; Heard et al., 2018) and represent a karstic carbonate aquifer shaped by microbial speleogenesis (Hochman, 2000). Therefore, oxic weathering and biological sulfide oxidation may surpass IROP in sulfate production. In contrast, the deep, high-temperature KL445 waters are highly reducing with abundant He and H_2 gases generated from radioactive decay of U and Th in the host rocks (Simkus et al., 2016). It would be reasonable if the dissolved sulfate were mostly produced by IROP as in the case of Kidd Creek (Li et al., 2016).

Oxygen isotope compositions of dissolved sulfate provide another tool to examine the sulfate production process. In contrast to sulfur isotopes, which generally show insignificant shift relative to their precursor sulfide in all the oxidation processes mentioned above (Toran and Harris, 1989; Balci et al., 2007; Pisapia et al., 2007; Lefticariu et al., 2010; Thurston et al., 2010), oxygen isotope compositions of sulfate strongly depend on the relative contribution of oxygen from H_2O and atmospheric O_2, which vary significantly among difffernt oxidation mechamisms (Lloyd, 1967). A compilation of $\delta^{18}O_{Sulfate}$ and $\delta^{18}O_{H2O}$ data from both biotic and abiotic sulfide oxidation reactions by a number of experimental studies and theoretical calculations is illustrated in Fig. 5. Most of the biotic and abiotic data spread over the same range between the two lines defined by (1) 100% oxygen in sulfate from water (hereafter referred as the 100% H_2O line) and (2) oxygen in sulfate equally from water and atmospheric O_2 (hereafter

referred as the 50:50 line). It is thus difficult to unambiguously distinguish between biotic and abiotic sulfide oxidation processes based on sulfur and oxygen isotopic signatures alone (Toran and Harris, 1989; Balci et al., 2007). The data from IROP experiments (Lefticariu et al., 2010) sit closely to the 100% H_2O line (Fig. 5), consistent with a single oxygen source from H_2O under anaerobic conditions.

Among the studied samples, the low-temperature DR5IPC and DR9IPC samples sit between the two lines in Figure 5, but closer to the 50:50 line, suggesting that sulfide oxidation in these fracture waters could have occurred in the presence of free O_2. This is consistent with the IROP modeling results suggesting that oxidative sulfide weathering is likely responsible for most of the dissolved sulfate in the Driefontein fracture waters. In contrast, the data of JO129 and TT118 are closer to the 100% H_2O line, suggesting that the sulfate production in these fracture systems may be dominated by anaerobic sulfide oxidation and/or IROP. It is interesting to see that the KL445 data lie slightly above the 50:50 line rather than close to the 100% H_2O line as expected (Fig. 5). This discrepancy can be explained by oxygen isotope exchange between dissolved sulfate and its host water (see Sections 4.4) and/or BSR (see Section 4.5). The samples from TT107 and TT109 also fall on the 50:50 line. Because of the relatively recent (within the last ~20 kyr from ^{14}C analyses; Simkus et al., 2016) surface meteoric water recharge into the TT107 fracture system, it is likely oxidative sulfide weathering play an important role in these systems.

4.4. Sustainability of sulfate production

The timescale (e.g., episodic or continuous) of sulfate supply from sulfide oxidation in the fracture systems is important to evaluate the nutrient sustainability for the microbial ecosystems in these long-isolated systems. Because of the active sulfur recycling processes (e.g.,

BSR) ongoing in the fracture water systems, it is difficult to quantitatively derive the sulfate productivity and the timescale for sulfate production. Alternatively, the oxygen isotope exchange rate between dissolved sulfate and water is used as a reference to qualitatively constrain the timescale of sulfate production.

The rate constant of SO_4^{2-}–H_2O isotope exchange is dependent on temperature and pH conditions. Lloyd (1968) determined the oxygen isotope exchange rate constants at a variety of temperatures as low as 25 ºC at pH of 3.8, 7 and 9. Since the samples in this study have a pH range of 7.39-8.96 (except the TT108 sample, pH = 6.45; Table A.1), their oxygen isotope exchange rate constants can be bracketed by the temperature interpolated values at pH of 7 and 9 (Lloyd, 1968). Assuming a first-order reaction for the oxygen isotope exchange between the dissolved sulfate and host water (Lloyd, 1968) and a closed system (i.e., no sulfate loss or gain), the estimated times for 99% oxygen isotope exchange in the studied samples range between 1.9 to 10.7 kyr at pH = 7 and 9.3 to 37.6 kyr at pH = 9 (Table A.2). These numbers are at least an order of magnitude less than the residence times determined by noble gas from either the same fracture systems (i.e., TT107, DR5IPC, and MM546; Heard et al., 2018) or fracture systems nearby (e.g., KL441, Lippmann et al., 2003; MP104, Lin et al., 2006). The estimated times for equilibrium isotope exchange are also within (i.e., TT107) or smaller than (i.e., TT109, DR5IPC) the range of ^{14}C ages (Table A.2). Therefore, SO_4^{2-}–H_2O oxygen isotope equilibration is expected if sulfate was externally produced and episodically supplied to the fracture waters before the systems were closed.

Fig. 6 illustrates the oxygen isotopic data of dissolved sulfate and their host waters in reference to the equilibration lines. While the Kloof samples and most of the Tau Tona samples are close to oxygen isotope equilibration, the data of the DR5IPC, DR9IPC, TT118, and JO129

samples are far below the isotope equilibration lines (Halas and Pluta, 2000; Zeebe, 2010). Despite that BSR can elevate the $\delta^{18}O$ of remaining dissolved sulfate (Fig. 6), the lack of isotope equilibration at these sites implies that the sulfate production has been maintained after these fractures were isolated, and that the sulfate productivity over the last tens of thousand years is high enough to overwhelm the isotopic effects from SO_4^{2-}–H_2O isotope exchange and BSR. In contrast, the data of the KL445, TT107 and TT109 samples sit very close to the isotope equilibration lines (Fig. 6). For the TT107 and TT109 samples, the dissolved sulfide concentrations are one to three orders in magnitude lower than the dissolved sulfide concentrations (Table A.1), and the $\delta^{34}S$ values of dissolved sulfate (3.3‰ to 5.5‰) are not significantly elevated, indicating that the BSR effects in these samples are not significant. Thus their high $\delta^{18}O$ values may be attributed to isotope equilibration with host waters or significant incorporation of atmospheric O_2 during sulfate formation – the 50:50 line from sulfide oxidation in Fig. 5 is accidently close to the equilibration lines in Fig. 6. For the KL445 samples, their highly reducing conditions can exclude the effect from incorporation of atmospheric O_2 during sulfate formation. The high $\delta^{34}S_{Sulfate}$ values (19.0‰ to 19.4‰) however indicate relatively high degree of BSR, which may at least partially account for the high $\delta^{18}O_{Sulfate}$ values, besides the effect from SO_4^{2-}–H_2O isotope exchange. Nevertheless, the state of near oxygen isotope equilibration of these samples implies that the sulfate production over the last few thousand years has not been efficient enough to overwhelm the effects from oxygen isotope exchange and/or BSR. This further suggests an inefficient sulfide oxidation process (e.g., IROP) has been dominating these fracture water systems.

4.5. Microbial activities in the subsurface fracture waters

The multiple sulfur isotope compositions of dissolved sulfide were also obtained for 8 out of the 14 samples. The results (Table 1) show that the sulfides are more depleted in ^{34}S (by 3.0‰ to 26.4‰) relative to the coexisting dissolved sulfate, but have more or less consistent $\Delta^{33}S$ values (a difference within 0.2‰ despite of a large $\Delta^{33}S$ range from –0.40‰ tp +0.50‰; Table 1; Fig. 7A; see more discussions below). These features are consistent with BSR, which is further corroborated by the widespread occurrence of sulfate reducing bacteria in the studies waters (e.g., Gihring et al. 2006; Lau et al. 2014; Magnabosco et al. 2015; Simkus et al. 2016; Stepanauskas et al., 2021). Unfortunately, given that BSR induced sulfur isotope fractionations can vary significantly among different sulfate-reducing bacteria (e.g., Sim et al., 2011) and different conditions (Habicht et al., 2002), the lack of constraint on sulfur isotope fractionations by the sulfate-reducing bacteria in the deep subsurface conditions of the Witwatersrand Basin impedes a quantitative modeling of BSR in these fracture systems.

Although the first-order isotopic signatures of dissolved sulfide and sulfate appear to be controlled by BSR, some samples display notable $\Delta^{33}S$ discrepancies between dissolved sulfide and sulfate (up to 0.18‰; Table 1; Fig. 7). To examine whether these discrepancies can be attributed to BSR, we compared the data with the BSR-induced $\Delta^{33}S$ shifts predicted by Johnston et al. (2007). Compared with the modeling results using sulfur isotope fractionation factors at 20 ºC (the lower temperature limit of our samples) (Fig. 7B), most of the samples fall in (within error) or close to the boundary of the BSR domain on the $\Delta^{33}S_{sulfide\text{-}sulfate}$ –$\Delta^{34}S_{sulfide\text{-}sulfate}$ diagram (Fig. 7B), but two samples (TT107 and MP120) are out of range. A closer look at the data suggest that the dissolved sulfate in the Tau Tona samples show relatively stable $\Delta^{33}S$ values, whereas dissolved sulfide show more variable $\Delta^{33}S$ values. Accordingly, we speculate that the sulfide in some of the fracture waters, which are mostly at low abundance and susceptible to

disturbance, were likely altered by mixing with a secondary dissolved sulfide. Seismic opening of the fracture systems (e.g., Sherwood Lollar et al., 2007), which could have occurred more recently either naturally or mining-related, could introduce secondary dissolved sulfide with a different $\Delta^{33}S$ value.

Bacterial sulfate reduction may affect the oxygen isotope compositions of the remaining sulfate due to associated kinetic isotope fractionations, typically on the order of 0-5‰ (e.g., Brunner et al., 2005; Turchyn et al., 2010; Antler et al., 2017). Using the upper limit of 5‰, the $\delta^{18}O$ shift of the remaining sulfate estimated by a batch model is shown on Fig. 6. It should be noted that the $\delta^{34}S$ values of dissolved sulfate in most of the studied samples (including those from Tau Tona) are < 7‰ and are within the $\delta^{34}S$ range of sulfide minerals in host rocks (Fig. 4). Thus, BSR in these samples and its effect on $\delta^{18}O$ should be minor. The KL445 samples and the MP120 sample show significantly elevated $\delta^{34}S$ values (17.2‰ to 19.4‰), which can be a result of relatively large extents of BSR reaction. This is supported by a recent genomic study on the MP120 sample showing that all 66 single-cell amplified genomes are affiliated to the sulfate-reducing bacterium *Cadidatus* Desulforudis audaxviator (Becraft et al., 2021).

5. Conclusions

Combined multiple sulfur isotope and oxygen isotope data of 14 fracture water samples from 6 gold mines in the Witwatersrand Basin suggest that ongoing in situ oxidation of sulfide minerals in host rocks supplies dissolved sulfate to the fracture water systems and contributes to sustaining a subsurface biosphere to depths > 3 km. At less than 1 km depth, where fracture waters retain an aerobic to microaerophilic character, the sulfate is likely predominantly generated by oxidative weathering of sulfide minerals, either biologically or abiotically. In

contrast, in deep (1-3 km) anaerobic fracture waters, the sulfate contains a significant fraction likely sourced from indirect radiolytic oxidation of sulfide. In both cases, the deep sulfur recycling with geologically driven sulfate production in situ can provide a long-term (on geological time scales) steady source of electron acceptor to support microbial ecosystems in subsurface water systems, at least at the maintenance level. Accordingly, availability of sulfate as a terminal electron acceptor would not be the limiting factor for the spatial expansion of the terrestrial subsurface biosphere, as long as temperature allows.

Acknowledgements

This work was funded by the Sloan Foundation − Deep Carbon Observatory – Deep Life and Deep Energy projects and NSERC-Discovery Grant to LL, and the NSERC – Discovery Grant to BSL. We thank Dr. Louis Derry and Dr. Laurence Coogan for editorial handling and Dr. Yanan Shen and an anonymous reviewer for their constructive comments.

Reference

Antler , G., Turchyn, A.V., Ono, S., Sivan, O., Bosak, T., 2017. Combined ^{34}S, ^{33}S and ^{18}O isotope fractionations record different intracellular steps of microbial sulfate reduction. *Geochim. Cosmochim. Acta* **203**, 364-380.

Balci, N., Shanks, W.C., Mayer, B., Mandernack, K.W., 2007. Oxygen and sulfur isotope systematics of sulfate produced by bacterial and abiotic oxidation of pyrite. *Geochimica et Cosmochimica Acta* **71**, 3796-3811.

Balci, N., Mayer, B., Shanks, W.C., Mandernack, K.W., 2012. Oxygen and sulfur isotope systematics of sulfate produced during abiotic and bacterial oxidation of sphalerite and elemental sulfur. *Geochimica et Cosmochimica Acta* **77**, 335-351.

Beach, A., Smith, R., 2007. Structural geometry and development of the Witwatersrand Basin, South Africa. *Geological Society, London, Special Publications* **272**, 533-542.

Borgonie, G., Linage-Alvarez, B., Ojo, A.O., Mundle, S.O.C., Freese, L.B., Rooyen, C.V., Kuloyo, O., Albertyn, J., Pohl, C., Cason, E.D., Vermeulen, J., Pienaar, C., Litthauer, D., Niekerk, H.V., Eeden, J.V., Sherwood Lollar, B., Onstott, T.C., van Heerden, E., 2015. Eukaryotic opportunists dominate the deep-subsurface biosphere in South Africa. *Nature Communications* **6**, 8952-8963.

Brunner, B., Bernasconi, S.M., Kleikemper, J., Schroth, M.H., 2005. A model for oxygen and sulfur isotope fractionation in sulfate during bacterial sulfate reduction processes. *Geochim. Cosmochim. Acta* **69**, 4773-4785.

Brunner, B., Yu, J.Y., Mielke, R.E., MacAskill, J.A., Madzunkov, S., McGenity, T.J., Coleman, M., 2008. Different isotope and chemical patterns of pyrite oxidation related to lag and exponential growth phases of Acidithiobacillus ferrooxidans reveal a microbial growth strategy. *Earth and Planetary Science Letters* **270**, 63-72.

Chivian, D., Brodie, E.L., Alm, E.J., Culley, D.E., Dehal, P.S., DeSantis, T.Z., Gihring, T.M., Lapidus, A., Lin, L.-H., Lowry, S.R., Moser, D.P., Richardson, P.M., Southam, G., Wanger, G., Pratt, L.M., Andersen, G.L., Hazen, T.C., Brockman, F.J., Arkin, A.P., Onstott, T.C., 2008. Environmental genomics reveals a single-species ecosystem deep within Earth. *Science* **322**, 275-278.

Coward, M.P., Spencer, R.M., Spencer, C.E., 1995. Development of the Witwatersrand Basin, South Africa. *Geological Society, London, Special Publications* **95**, 243-269.

Dankert, B.T., Hein, K.A., 2010. Evaluating the structural character and tectonic history of the Witwatersrand Basin. *Precambrian Research* **177**, 1-22.

Edwards, C.T., Fike, D.A., Saltzman, M.R., 2019. Testing carbonate-associated sulfate (CAS) extraction methods for sulfur isotope stratigraphy: A case study of a Lower–Middle Ordovician carbonate succession, Shingle Pass, Nevada, USA. *Chem. Geol.* **529**, 119297.

Farquhar, J., Bao, H., Thiemens, M., 2000. Atmospheric influence of Earth's earliest sulfur cycle. *Science* **289**, 756-758.

Frimmel, H. E., 2005. Archaean atmospheric evolution: evidence from the Witwatersrand gold fields, South Africa. *Earth-Science Reviews* **70**, 1–46.

Gartz, V.H., Frimmel, H.E., 1999. Complex Metasomatisom of an Archean Placer in the Witwatersrand Basin, South Africa: The Ventersdor Contact Reef – A Hydrothermal Aquifer? *Econ. Geol.* **94**, 689-706.

Gihring, T.M., Moser, D.P., Lin, L.-H., Davidson, M., Onstott, T.C., Morgan, L., Milleson, M., Kieft, T.L., Trimarco, E., Balkwill, D.L., Dollhopf, M.E., 2006. The distribution of

microbial taxa in the subsurface water of the Kalahari Shield, South Africa. *Geomicrobiol. J.* **23**, 415–430

Guy, B., 2012. Pyrite in the Mesoarchean Witwatersrand Supergroup, South Africa. PhD thesis. University of Johannesburg. Pp 492.

Guy, B., Ono, S., Gutzmer, J., Kaufman, A., Lin, Y., Fogel, M., Beukes, N., 2012. A multiple sulfur and organic carbon isotope record from non-conglomeratic sedimentary rocks of the Mesoarchean Witwatersrand Supergroup, South Africa. *Precambrian Research* **216**, 208-231.

Guy, B.M., Ono, S., Gutzmer, J., Lin, Y., Beukes, N.J., 2014. Sulfur sources of sedimentary "buckshot" pyrite in the Auriferous Conglomerates of the Mesoarchean Witwatersrand and Ventersdorp Supergroups, Kaapvaal Craton, South Africa. *Mineral. Deposita* **49**, 751-775.

Habicht, K.S., Gabe, M., Thamdrup, B., Berg, P., Canfield, D.E., 2002. Calibration of sulfate levels in the Archean ocean. *Science* **298**, 2372-2374.

Halas, S., Pluta, I., 2000. Empirical calibration of isotope thermometer of $\delta^{18}O(SO_4^{2-})$-$\delta^{18}O(H_2O)$ for low temperature brines. V Isotope Workshop, European Society for Isotope Research, Kraków, Poland, 68-71.

Hallbeck L, Pedersen K (2008) Characterization of microbial processes in deep aquifers of the Fennoscandian Shield. Applied Geochemistry 23:1796-1819.

Heard, A.W., Warr, O., Borgonie, G., Linage, B., Kuloyo, O., Fellowes, J.W., Magnabosco, C., Lau, M.C.Y., Erasmus, M., Cason, E.D., van Heerden, E., Kieft, T.L., Mabry, J.C., Onstott, T.C., Sherwood Lollar, B., Ballentine, C.J., 2018. South African crustal fracture fluids preserve paleometeoric water signatures for up to tens of millions of years. *Chem. Geol.* **493**, 379-395.

Hochman, M. 2000. A Case for Biotic Speleogenesis in a Dolomite Aquifer in South Africa. BA Thesis. Dept. of Geosciences, Princeton University, 132 pp.

Hofmann, A., Bekker, A., Rouxel, O., Rumble, D., Master, S., 2009. Multiple sulphur and iron isotope composition of detrital pyrite in Archaean sedimentary rocks: A new tool for provenance analysis. *Earth and Planetary Science Letters* **286**, 436-445.

Johnson, J.E, Gerpheide, A., Lamb, M.P., Fischer, W.W., 2014. O_2 constraints from Paleoproterozoic detrital pyrite and uraninite. *GSA Bullet.* **126**, 813-830.

Johnson, M., Van Vuuren, C., Hegenberger, W., Key, R., Show, U., 1996. Stratigraphy of the Karoo Supergroup in southern Africa: an overview. *Journal of African Earth Sciences* **23**, 3-15.

Johnston, D.T., Farquhar, J., Canfield, D.E., 2007. Sulfur isotope insights into microbial sulfate reduction: when microbes meet models. *Geochim. Cosmochim. Acta* **71**, 3929-3947.

Kampschulte, A., Bruckschen, P., Strauss, H., 2001. The sulphur isotopic composition of trace sulphates in Carboniferous brachiopods: implications for coeval seawater, correlation with other geochemical cycles and isotope stratigraphy. *Chemical Geology* **175**, 149-173.

Kietäväinen, R., Ahonen, L., Kukkonen, I.T., Hendriksson, N., Nyyssönen, M., Itävaara, M., 2013. Characterisation and isotopic evolution of saline waters of the Outokumpu Deep Drill Hole, Finland—implications for water origin and deep terrestrial biosphere. *Appl. Geochem.* **32**, 37–51.

Labonté, J., Field, E., Lau, M., Chivian, D., van Heerden, E., Wommack, K.E., Kieft, T.L., Onstott, T.C., Stepanauskas, R., 2015. Single cell genomics indicates horizontal gene transfer and viral infections in a deep subsurface Firmicutes population. Front. Microbiol. 6, 349. doi:10.1038/ismej.2015.48.

Lau, C.Y.M., Cameron, C., Magnabosco, C., Brown, C.T., Schilkey, F., Grim, S., Hendrickson, S., Pullin, M., Lacrampe-Couloume, G., Sherwood Lollar, B., van Heerden, E., Kieft, T.L., Onstott, T.C., 2014. Phylogeny and phylogeography of functional genes shared among seven terrestrial subsurface metagenomes reveal N-cycling and microbial evolutionary relationships. *Front. Microbiol.* **5**, 531. doi: 10.3389/fmicb.2014.00531.

Lau, M.C.Y., Kieft, T.L., Kuloyo, O., Linage, B., van Heerden, E., Lindsay, M.R., Magnabosco, C., Wang, W., Wiggins, J.B., Guo, L., Perlman, D.H., Kyin, S., Shwe, H.H., Harris, R.L., Oh, Y., Yi, M.J., Purtschert, R., Slater, G.F., Ono, S., Wei, S., Li, L., Sherwood Lollar, B., Onstott, T.C., 2016. Deep-subsurface community dependent on syntrophy is dominated by sulfur-driven autotrophic denitrifiers. *PNAS* **113**, E7927–E7936.

Lefticariu, L., Pratt, L.M., LaVerne, J.A., Schimmelmann, A., 2010. Anoxic pyrite oxidation by water radiolysis products - A potential source of biosustaining energy. *Earth Planet. Sci. Lett.* **292**, 57-67.

Li, L., Wing, B.A., Bui, T.H., McDermott, J.M., Slater, G.F., Wei, S., Lacrampe-Couloume, G., Sherwood Lollar, B., 2016. Sulfur mass-independent fractionation in subsurface fracture waters indicates a long-standing sulfur cycle in Precambrian rocks. *Nature Communications* **7**, 1325.

Lin, L.-H., Hall, J.A., Lippmann, J.,Ward, J., Sherwood Lollar, B., DeFlaun, M., Rothmel, R., Moser, D.P., Gihring, T.M., Mislowack, B., Onstott, T.C., 2005a. Radiolytic H_2 in continental crust: Nuclear power for deep subsurface microbial communities. *Geochem. Geophys. Geosyst.* **6**, Q07003.

Lin, L.-H., Slater, G.F., Sherwood Lollar, B., Lacrampe-Couloume, G., Onstott, T.C., 2005b. The yield and isotopic composition of radiolytic H_2, a potential energy source for the deep subsurface biosphere. *Geochim. Cosmochim. Acta* **69**, 893-903.

Lin, L.-H., Wang, P.-L., Lippmann-Pipke, J., Boice, E., Pratt, L.M., Sherwood Lollar, B., Brodie, E.L., Hazen, T.C., Andersen, G.L., DeSantis, T.Z., Moser, D., Kershaw, D., Onstott, T.C., 2006. Long-term sustainability of a high-energy, low-diversity crustal biome. *Science* **314**, 479-482.

Lippmann-Pipke, J., Sherwood Lollar, B., Niedermann, S., Stroncik, N.A., Naumann, R., van Heerden, E., Onstott, T.C., 2011. Neon identifies two billion year old fluid component in Kaapvaal Craton. *Chem. Geol.* **283**, 287-296.

Lippmann, J., Stute, M., Torgersen, T., Moser, D.P., Hall, J.A., Lin, L.-H., Borcsik, M., Bellamy, R.E.S., Onstott, T.C., 2003. Dating ultra-deep mine waters with noble gases and ^{36}Cl, Witwatersrand Basin, South Africa. *Geochim. Cosmochim. Acta* **67**, 4597-4619.

Lloyd, R.M., 1968. Oxygen isotope behavior in the sulfate-water system. *Journal of Geophysical Research* **73**, 6099-6110.

Lollar, G.S., Warr, O., Telling, J., Osburn, M.R., Sherwood Lollar, B., 2019. 'Follow the Water': hydrogeochemical constraints on microbial investigations 2.4 km below surface at the Kidd Creek Deep Fluid and Deep Life Observatory. *Geomicrobiol. J.* **36**, 859-872.

Magnabosco, C., Ryan, K., Lau, C.Y.M., Kuloyo, O., Sherwood Lollar, B., Kieft, T., van Heerden, E., onstott, T.C., 2015. A metagenomic window into carbon metabolism at 3 km depth in Precambrian Continental Crust. *The ISME Journal* **10**, 730-741.

Magnabosco, C., Timmers, P.H.A., Lau, M.C.Y., Borgonie, G., Linage-Alvarez, B., Kuloyo, O., Alleva, R., Kieft, T.L., Slater, G.S., van Heerden, E., Sherwood Lollar, B., Onstott, T.C., 2018. Fluctuations in populations of subsurface methane oxidizers in coordination with

changes in electron acceptor availability. *FEMS Microbiology Ecology* **94**, doi: 10.1093/femsec/fiy1089.

Martin, D.M., Clendenin, C., Krapez, B., McNaughton, N., 1998. Tectonic and geochronological constraints on late Archaean and Palaeoproterozoic stratigraphic correlation within and between the Kaapvaal and Pilbara Cratons. *Journal of the Geological Society* **155**, 311-322.

Mazor, E., Verhagen, B.T., 1983. Dissolved ions, stable and radioactive isotopes and noble gases in thermal waters of South Africa. *J. Hydrol.* **63**, 315-329.

Moser, D.P., Onstott, T.C., Fredrickson, J.K., Brockman, F.J., Balkwill, D.L., Drake, G.R., Pfiffner, S., White, D.C., Takai, K., Pratt, L.M., Fong, J., Sherwood-Lollar, B., Slater, G., Phelps, T.J., Spoelstra, N., DeFlaun, M., Southam, G., Welty, A.T., Baker, B.J., Hoek, J., 2003. Temporal shifts in Microbial Community Structure and Geochemistry of an Ultradeep South African Gold Mine Borehole. *Geomicrobiol. J.* **20**, 517-548.

Ono, S., Eigenbrode, J.L., Pavlov, A.A., Kharecha, P., Rumble, D., Kasting, J.F., Freeman, K.H., 2003. New insights into Archean sulfur cycle from mass-independent sulfur isotope records from the Hamersley Basin, Australia. *Earth and Planetary Science Letters* **213**, 15-30.

Ono, S., Keller, N.S., Rouxel, O.J., Alt, J.C., 2012. Sulfur-33 constraints on the origin of secondary pyrite in altered oceanic basement. *Geochim. Cosmochim. Acta* **87**, 323-340.

Onstott, T.C., Moser, D.P., Fredrickson, J.K., Brockman, F.J., Pfiffner, S.M., Phelps, T.J., White, D.C., Peacock, A., Balkwill, D., Hoover, R., Krumholz, L.R., Borscik, M., Kieft, T.L., Wilson, R.B., 2003. Indigenous versus contaminant microbes in ultradeep mines. *Environ. Microbiol.* **5**, 1168-1191.

Onstott, T.C., Lin, L.-H., Davidson, M., Mislowack, B., Borcsik, M., Hall, J., Slater, G.F., Ward, J.A., Sherwood Lollar, B., Lippmann-Pipke, J., Boice, E., Pratt, L.M., Pfiffner, S., Moser, D.P., Gihring, T.M., Kieft, T.L., Phelps, T.J., van Heerden, E., Litthaur, D., DeFlaun, M., Rothmel, R., Wanger, G., Southam, G., 2006. The origin and age of biogeochemical trends in deep fracture water of the Witwatersrand Basin, South Africa. *Geomicrobiol. J.* **23**, 369-414.

Onstott, T.C., McGown, D.J., Bakermans, C., Ruskeeniemi, T., Ahonen, L., Telling, J., Boettiger, C., Ho, R., Soffientino, B., Pfiffner, S.M., DiFurio, S., Sherwood Lollar, B., Frape, S., Stotler, R., Johnson, E.J., Vishnivetskaya, T.A., Rothmel, R., Pratt, L.M., 2009. Microbial communities in subpermafrost saline fracture water at the Lupin Au mine, Nunavut, Canada. *Microb. Ecol.* **58**, 786-807.

Pedersen K, Bengtsson AF, Edlund JS, Eriksson LC (2014) Sulphate-controlled Diversity of Subterranean Microbial Communities over Depth in Deep Groundwater with Opposing Gradients of Sulphate and Methane. Geomicrobiology Journal 31:617–631.

Pellerin, A., Antler, G., Holm, S.A., Findlay, A.J., Crockford, P.W., Turchyn, A., Jørgensen, B.B., Finster, K., 2019. Large sulfur isotope fractionation by bacterial sulfide oxidation. *Sci. Adv.* **5**, eaaw1480.

Pisapia, C., Chaussidon, M., Mustin, C., Humbert, B., 2007. O and S isotopic composition of dissolved and attached oxidation products of pyrite by Acidithiobacillus ferrooxidans: comparison with abiotic oxidations. *Geochimica et Cosmochimica Acta* **71**, 2474-2490.

Purkamo, L., Bomberg, M., Nyyssönen, M., Ahonen, L., Kukkonen, I., Itävaara, M. (2017) Response of Deep Subsurface Microbial Community to Different Carbon Sources and Electron Acceptors during 2 months Incubation in Microcosms. *Front. Microbiol.* **8**, 232.

Qureshi, R.M., 1987. The isotopic composition of aqueous sulfate: a laboratory investigation. Ph.D. Thesis, University of Waterloo.

Robb, L.J., Meyer, F.M., 1995. The Witwatersrand Basin, South Africa: geological framework and mineralization processes. *Ore Geology Reviews* **10**, 67-94.

Schwarcz, H.P., Cortecci, G., 1974. Isotopic analyses of spring and stream water sulfate from the Italian Alps and Apennines. *Chem. Geol.* **13**, 285-294.

Seal, R.R., 2006. Sulfur isotope geochemistry of sulfide minerals. *Rev. Mineral. Geochem.* **61**. Mineralogical Society of America, pp. 633-677.

Sherwood Lollar, B., Lacrampe-Couloume, G., Slater, G., Ward, J., Moser, D., Gihring, T., Lin, L.-H., Onstott, T., 2006. Unravelling abiogenic and biogenic sources of methane in the Earth's deep subsurface. *Chemical Geology* **226**, 328-339.

Sherwood Lollar, B., Voglesonger, K., Lin, L.-H., Lacrampe-Couloume, G., Telling, J., Abrajano, T., Onstott, T., Pratt, L., 2007. Hydrogeologic controls on episodic H2 release from Precambrian fractured rocks-Energy for deep subsurface life on Earth and Mars. *Astrobiology* **7**, 971-986.

Sim, M.S., Bosak, T., Ono, S., 2011. Large sulfur isotope fractionation does not require disproportionation. *Science* **333**, 74-77.

Simkus, D.N., Slater, G.F., Sherwood Lollar, B., Wilkie, K., Kieft, T.L., Magnabosco, C., Lau, M.C.Y., Pullin, M.J., Hendrickson, S.B., Wommack, K.E., Sakowski, E.G., van Heerden, E., Kuloyo, O., Linage, B., Borgonie, G., Onstott, T.C., 2016. Variations in microbial carbon sources and cycling in the deep continental subsurface. *Geochim. Cosmochim. Acta* **173**, 264-283.

Becraft, E., Lau, M.C.Y., Bezuidt, O., Brown, J., Labonté, J., Kauneckaite-Griguole, K., Salkauskaite, R., Alzbutas, G., Sackett, J., Kruger, B., Moser, D., Kadnikov, V., Ravin, N., Onstott, T., van Heerden, E., and Stepanauskas, R. (2021) Evolutionary stasis of a deep subsurface microbial lineage. *The ISME J*. https://doi.org/10.1038/s41396-021-00965-3.

Takai, K., Moser, D.P., DeFlaun, M., Onstott, T.C., Fredrickson, J.K., 2001. Archaeal diversity in waters from deep South African gold mines. *Appl. Environ. Microbiol.* **67**, 5750-5760.

Taylor, B.E., Wheeler, M.C., Nordstrom, D.K., 1984. Stable isotope geochemistry of acid mine drainage: Experimental oxidation of pyrite. *Geochimica et Cosmochimica Acta* **48**, 2669-2678.

Thurston, R.S., Mandernack, K.W., Shanks III, W.C., 2010. Laboratory chalcopyrite oxidation by Acidithiobacillus ferrooxidans: oxygen and sulfur isotope fractionation. *Chemical Geology* **269**, 252-261.

Toran, L., Harris, R.F., 1989. Interpretation of sulfur and oxygen isotopes in biological and abiological sulfide oxidation. *Geochimica et Cosmochimica Acta* **53**, 2341-2348.

Turchyn, A.V., Brochert, V., Lyons, T.W., Engel, G.S., Balci, N., Schrag, D.P., Brunner, B., 2010. Kinetic oxygen isotope effects during dissimilatory sulfate reduction: a combined theoretical and experimental approach. *Geochim. Cosmochim. Acta* **74**, 2011-2024.

van Everdingen, R.O., Krouse, H.R., 1988. Interpretation of isotopic compositions of dissolved sulfate in acid mine drainage. *Technical Reports*, https://zone.biblio.laurentian.ca/bitstream/10219/13033/10211/SB10099.pdf.

Vovk, I.F., 1987. Radiolytic oxidation of sulphides and geochemical behavior of sulfur isotopes in uranium deposits. In: Studies on Sulphur Isotope Variations in Nature. International Atomic Energy Agency, Vienna, Austria, pp. 85–103.

Ward, J., Slater, G., Moser, D., Lin, L.-H., Lacrampe-Couloume, G., Bonin, A., Davidson, M., Hall, J., Mislowack, B., Bellamy, R., 2004. Microbial hydrocarbon gases in the

Witwatersrand Basin, South Africa: implications for the deep biosphere. *Geochimica et Cosmochimica Acta* **68**, 3239-3250.

Warr, O., Giunta, T., Onstott, T.C., Kieft, T., Harris, R.L., Nisson, D.M., Sherwood Lollar, B., 2021. The role of low-temperature 18O exchange in the isotopic evolution of deep subsurface fluids. *Chem. Geol.* **561**, 120027.

Watanabe, Y., Farquhar, J., Ohmoto, H., 2009. Anomalous fractionations of sulfur isotopes during thermochemical sulfate reduction. *Science* **324**, 370-373.

Zeebe, R.E., 2010. A new value for the stable oxygen isotope fractionation between dissolved sulfate ion and water. *Geochimica et Cosmochimica Acta* **74**, 818-828.

Figure captions

Fig. 1. Geological map of the studied area (right; modified from Dankert and Hein, 2010) and stratigraphic sequence of the Witwatersrand Basin (left; modified from Beach and Smith, 2007). Note that the Karoo Supergroup does not appear in this map. Yellow areas represent five major gold fields (Evander, Heidelberg, Carletonville, Klerksdorp and Welkom). Subsurface fracture water samples in this study were mainly collected from the Carletonville and Welkom regions, including deep fracture waters from the Kloof, Tau Tona and Mponeng gold mines, while shallower fracture waters were from the Joel, Masimong and Driefontein gold mines. KL = Kloof, TT = Tau Tona, MP = Mponeng, DR = Driefontein, JO = Joel, MM = Masimong.

Fig. 2. $\delta^{18}O$ versus $\delta^{2}H$ diagram of fracture water samples. Error bars of data are smaller than symbol size. For comparison, Global Meteoric Water Line (GMWL), Local Meteoric Water Line (LMWL; Mazor and Verhagen, 1983), previous fracture water samples from the Kloof, Tau Tona, Mponeng, Driefontein and Masimong gold mines (Onstott et al., 2006), modern mean annual precipitation from Pretoria, SA (filled circle) and saline water from Kidd Creek in Canadian Shield (Li et al., 2016) were also plotted. Sample abbreviations are the same as Fig. 1.

Figure 3. Diagram showing the $\delta^{34}S$ and $\Delta^{33}S$ of the dissolved sulfate in the subsurface fracture waters in the Witwatersrand Basin. For comparison, data of barite extracted from host rocks in the Mponeng mine (Lin et al., 2016) and carbonate-associated sulfate (CAS) in the Transvaal dolomite are also shown. Error bars of data are smaller than symbol size. Abbreviations are the same as in Fig. 1.

Figure 4. Comparison of multiple sulfur isotopic values for dissolved sulfate in fracture waters (this study) and sulfide minerals from the Witwatersrand Basin (Hofmann et al., 2009; Guy et al., 2012). Error bars of data are smaller than symbol size. Abbreviations are the same as in Fig. 1.

Fig. 5. Comparison of oxygen isotope compositions between dissolved sulfate and the expected range from oxidation of sulfide minerals. Sample abbreviations are the same as in Fig. 1. The $\delta^{18}O$ range of sulfate produced from sulfide oxidation is summarized from literature data (Schwarcz and Cortecci, 1974; Taylor et al., 1984; Qureshi, 1987; van Everdingen and Krouse, 1988; Balci et al., 2007; Pisapia et al., 2007; Brunner et al., 2008; Lefticariu et al., 2010; Thurston et al., 2010; Balci et al., 2012), which include experimental data for three oxidation mechanisms, abiotic sulfide oxidation (ASO), bacterial sulfide oxidation (BSO), and indirect radiolytic oxidation of pyrite (IROP). Some data with no identification of abiotic or bacterial oxidation are marked as "Unknown". The data in this study fall into the 50% and 100% H_2O lines, which intercept at the $\delta^{18}O$ value (24‰) of atmospheric O_2. See text for detailed discussion.

Fig. 6. Oxygen isotope fractionation versus temperature for the SO_4^{2-}-H_2O system. Solid lines are the equilibrium isotope fractionation lines by Halas and Pluta (2000) and Zeebe (2010). Error bars are smaller than symbol size. Sample abbreviations are the same as in Fig. 1. The effect of bacterial sulfate reduction (BSR) on $\delta^{18}O_{sulfate}$ is shown as an arrow for reference. The *F* numbers refer to the fraction of remaining sulfate after BSR.

Fig. 7. Comparison of absolute (A) and relative (B) $\delta^{34}S$ and $\Delta^{33}S$ values between coexisting dissolved sulfate and sulfide in fracture water samples. The data of dissolved sulfide and sulfate in the same sample are linked by a grey line in panel A. The grey curves in panel B outline the reference $\Delta^{33}S$ shifts caused by BSR predicted by the model of Johnston et al. (2007). Model temperature was set at 20 ºC, the lower temperature limit of the water samples in this study. Sample abbreviations are the same as in Fig. 1.

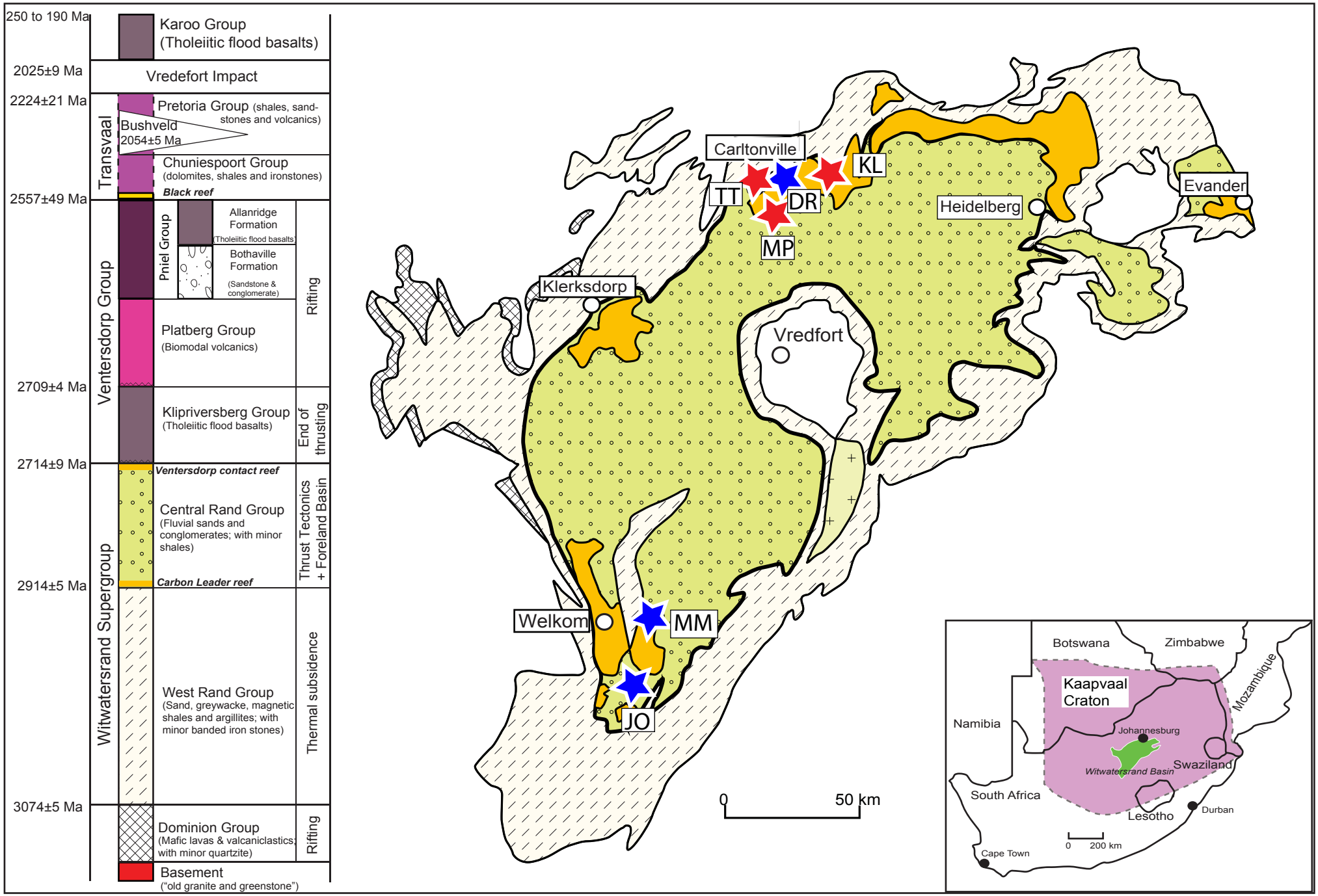
250 to 190 Ma
Karoo Group
(Tholeiitic flood basalts)
2025±9 Ma
Vredefort Impact
2224±21 Ma
Transvaal
Pretoria Group (shales, sandstones and volcanics)
Bushveld
2054±5 Ma
Chuniespoort Group
(dolomites, shales and ironstones)
Black reef
2557±49 Ma
Ventersdorp Group
Pniel Group
Allanridge Formation
(Tholeiitic flood basalts)
Bothaville Formation
(Sandstone & conglomerate)
Rifting
Platberg Group
(Biomodal volcanics)
2709±4 Ma
Klipriversberg Group
(Tholeiitic flood basalts)
End of thrusting
2714±9 Ma
Ventersdorp contact reef
Witwatersrand Supergroup
Central Rand Group
(Fluvial sands and conglomerates; with minor shales)
Thrust Tectonics + Foreland Basin
2914±5 Ma
Carbon Leader reef
West Rand Group
(Sand, greywacke, magnetic shales and argillites; with minor banded iron stones)
Thermal subsidence
3074±5 Ma
Dominion Group
(Mafic lavas & valcaniclastics; with minor quartzite)
Rifting
Basement
("old granite and greenstone")
Carltonville
KL
TT
DR
MP
Heidelberg
Evander
Klerksdorp
Vredfort
Welkom
MM
JO
0
50 km
Botswana
Zimbabwe
Mozambique
Kaapvaal Craton
Namibia
Johannesburg
Witwatersrand Basin
Swaziland
South Africa
Lesotho
Durban
Cape Town
0
200 km

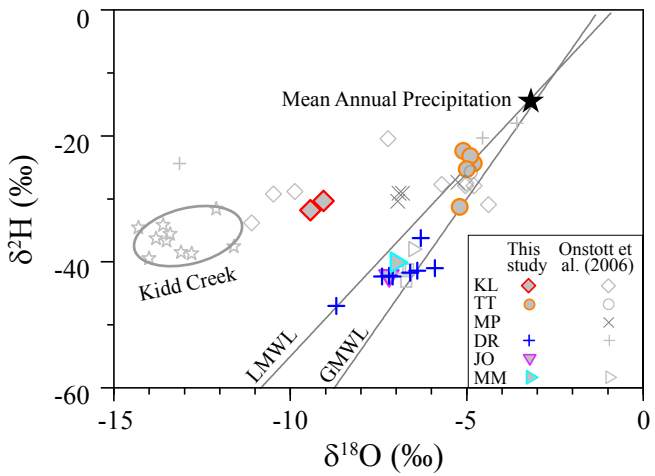
0
-20
-40
-60
-15
-10
-5
0
δ²H (‰)
δ¹⁸O (‰)
Mean Annual Precipitation
Kidd Creek
LMWL
GMWL
This study
Onstott et al. (2006)
KL
TT
MP
DR
JO
MM

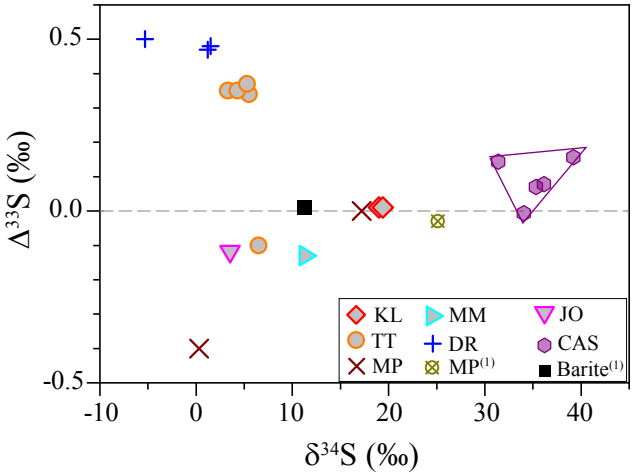
0.5
0.0
-0.5
-10
0
10
20
30
40
Δ33S (‰)
δ34S (‰)
KL
TT
MP
MM
DR
MP(1)
JO
CAS
Barite(1)

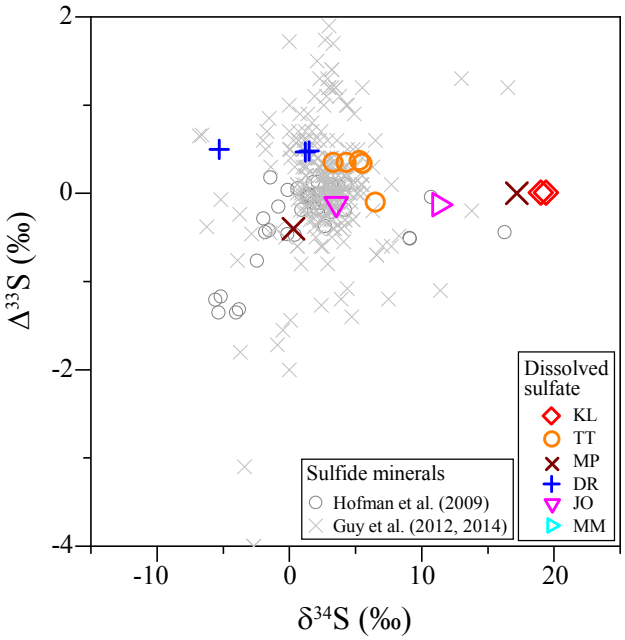
2
0
-2
-4
-10
0
10
20
Δ33S (‰)
δ34S (‰)
Sulfide minerals
Hofman et al. (2009)
Guy et al. (2012, 2014)
Dissolved sulfate
KL
TT
MP
DR
JO
MM

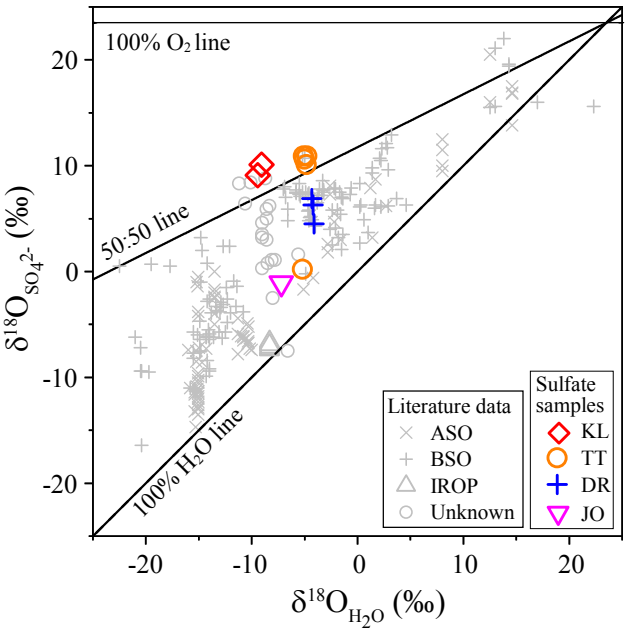
100% O2 line
50:50 line
100% H2O line
Literature data
ASO
BSO
IROP
Unknown
Sulfate samples
KL
TT
DR
JO
δ18OSO42- (‰)
δ18OH2O (‰)
20
10
0
-10
-20
-20
-10
0
10
20

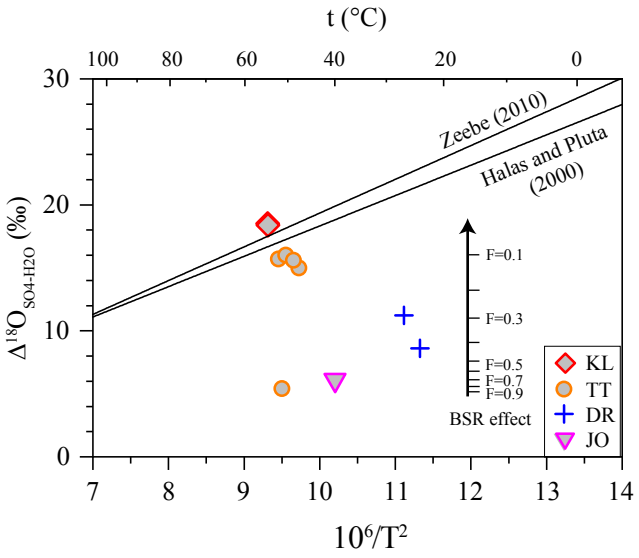
t (°C)
100
80
60
40
20
0
30
20
10
0
7
8
9
10
11
12
13
14
$10^6/T^2$
$\Delta^{18}O_{SO4-H2O}$ (‰)
Zeebe (2010)
Halas and Pluta (2000)
F=0.1
F=0.3
F=0.5
F=0.7
F=0.9
BSR effect
KL
TT
DR
JO

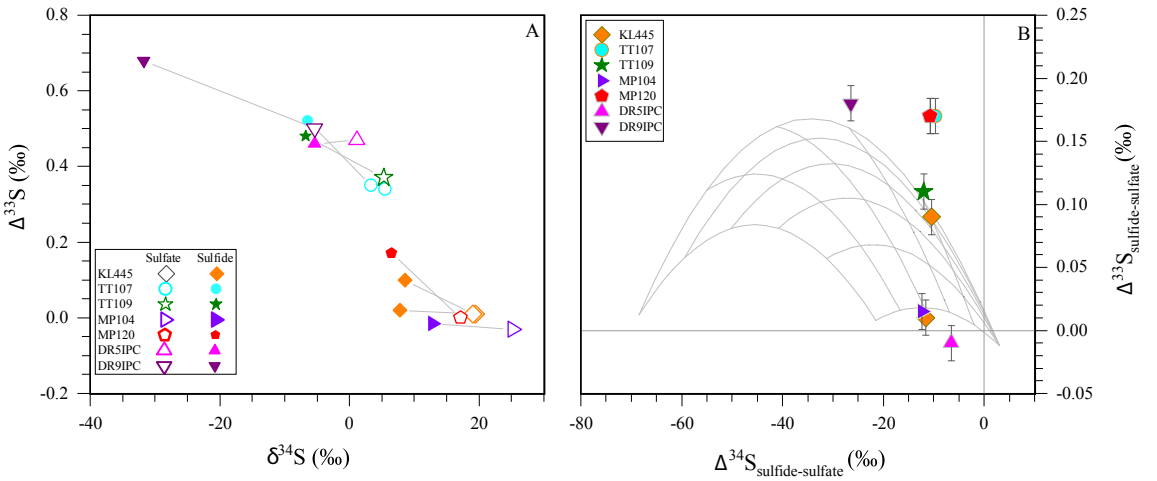
A
B
Sulfate
Sulfide
KL445
TT107
TT109
MP104
MP120
DR5IPC
DR9IPC
$\Delta^{33}S$ (‰)
$\delta^{34}S$ (‰)
$\Delta^{34}S_{sulfide-sulfate}$ (‰)
$\Delta^{33}S_{sulfide-sulfate}$ (‰)

Table 1. Isotope compositions of fracture water and dissolved sulfate and sulfide.

	H_2O		Sulfate				Sulfide			
Sample Name*	$\delta^{18}O$	$\delta^{2}H$	$\delta^{34}S$	$\Delta^{33}S$	$\delta^{18}O$	$\Delta^{18}O_{Sulfate-H2O}$	$\delta^{34}S$	$\Delta^{33}S$	$\Delta^{34}S_{Sufide-sulfate}$	$\Delta^{33}S_{Sufide-}$ $\Delta^{33}S_{Sulfate}$
KL445FW190711	-9.1	-30.3	19.4	0.01	9.3	18.4	7.8	0.02	-11.6	0.01
KL445FW280711	-9.4	-31.8	19.0	0.01	9.1	18.5	8.6	0.10	-10.4	0.09
TT107FW110811	-4.8	-24.4	3.3	0.35	10.9	15.7	-6.4	0.52	-9.7	0.17
TT107FW240811	-5.1	-22.4	5.5	0.34	10.9	16.0	n.d.	n.d.		
TT109FW190112	-4.9	-23.2	4.3	0.35	10.1	15.0	n.d.	n.d.		
TT109FW090212	-5.0	-25.3	5.3	0.37	10.6	15.6	-6.7	0.48	-12.0	0.11
TT118FW080212	-5.2	-31.3	6.5	-0.10	0.2	5.4	n.d.	n.d.		
MP99FW220514	n.s.	n.s.	0.3	-0.40	10.1		n.d.	n.d.		
MP120FW100614	n.s.	n.s.	17.2	0.00	8.2		6.5	0.17	-10.7	0.17
DR5IPCFW150711	-4.4	-24.3	1.5	0.48	6.9	11.3	n.d.	n.d.		
DR5IPCFW280711	-4.2	-24.9	1.2	0.47	6.3	10.5	-5.3	0.46	-6.5	-0.01
DR9IPCFW200112	-4.1	-19.8	-5.3	0.50	4.5	8.6	-31.7	0.68	-26.4	0.18
JO129FW250412	-7.2	-42.2	3.5	-0.12	-1.1	6.1	n.d.	n.d.		
MM546FW290612	-7.0	-40.1	11.3	-0.13	n.d.		8.3	n.d.	-3.0	

*Sample Name is expressed as “Mine Name + Shaft No. + Level No. + FW(=fracture water) + Collection Date (DD.MM.YY.)”.

KL=Kloof; TT=Tau Tona; MP=Mponeng; DR=Driefontein; JO=Joel; MM=Masimong.

n.s. = not sampled

n.d. = no data, because the sample amount is too low for isotopic analysis

Table 2. Multiple sulfur isotope compositions of various sulfur components in the Transvaal dolomites from the Driefontein gold mine.

Sample ID	**Component***	**$\delta^{34}S$**	**$\Delta^{33}S$**	**$\Delta^{36}S$**
DR-IPC5-01	Sulfate after H_2O_2	14.7	4.22	-4.0
	CAS	39.2	0.16	1.9
DR-IPC5-02	Sulfate after H_2O_2	10.6	3.32	-3.2
	CAS	31.4	0.14	3.4
	Insolvable remnant	2.3	2.66	-2.1
DR-IPC5-03	Sulfate after H_2O_2	8.3	2.65	-2.5
	CAS	36.2	0.08	-2.1
DR-IPC5-04	CAS	35.3	0.07	2.6
DR-IPC5-05	CAS	34.1	-0.01	3.0

* One or more components were extracted from the samples for multiple sulfur isotopic analysis. “Sulfate after H_2O_2” refers to the dissolved sulfate extracted from treatment of bulk-rock powders by 30% H_2O_2 for 48 hours. The sulfate in this step may be formed by oxidation of sulfide minerals and organic matter (if there is any); “CAS” refers to carbonate associated sulfate extracted from subsequent treatment of carbonate by 6N HCl for 6 hours; “Insolvable remnant” refers to the refractory material that was not dissolved by above treatments.

Appendix

Table A.1. Geochemistry of fracture waters from the Kloof, Tau Tona, Mponeng, Driefontein, Joel and Masimong mines.

Sample Name	**KL445 FW 190711**	**KL445 FW 280711**	**TT107 FW 110811**	**TT107 FW 240811**	**TT109 FW 190112 BH1**	**TT109 FW 080212 BH2**	**TT118 FW 0070112**	**MP99 FW 220514**	**MP120 FW 100614**	**DR5IPC FW 150711**	**DR5IP CFW 280711**	**DR9IPC FW 200112**	**JO129 FW 250412**	**MM546 FW 290612**
Location (Lat., Long.)	26.435° S 27.623° E		26.417° S 27.427° E					26.438° S 27.428° E	26.438° S 27.431° E	26.420° S 27.504° E		26.420° S, 27.482° E	28.278° S, 26.814° E	27.976° S 26.875° E
Depth(mbls)	3276		3048		3136		3413	n.m.	3402	1046		900	1300	1900
Host rock	Ventersdorp metavolcanics		Witwatersrand quartzite					Ventersdorp metavolcanics		Transvaal dolomite			Witwatersrand quartzite	
pH	8.00	n.m.	8.57	8.69	8.87	8.19	6.45	8.56	8.24	7.39	n.m.	8.8	8.96	7.71
T (°C)	54.5	n.m.	52.1	50.4	47.5	48.7	51.3	44.5	65.0	26.8	n.m.	24.0	39.9	40.7
Eh (mV SHE)	-51.5	n.m.	-45.6	-132.8	373.6	-62.3	129.8	-92.2	-89.2	n.m.	n.m.	68.7	217.1	53.5
Cl- (M)	1.97E-01	n.m.	2.79E-03	n.m.	n.m.	3.15E-03	1.29E-02	8.32E-03	2.14E-02	1.39E-03	n.m.	9.14E-04	6.60E-02	5.50E-02
Br- (M)	4.38E-04	n.m.	5.63E-06	n.m.	n.m.	6.92E-06	2.98E-05	1.66E-05	4.00E-05	2.63E-06	n.m.	1.15E-06	2.99E-04	1.60E-04
SO_4^{2-} (M)	9.85E-05	n.m.	1.04E-04	n.m.	n.m.	1.03E-04	1.17E-03	4.94E-04	n.m.	1.38E-04	n.m.	6.40E-04	3.67E-04	7.03E-06
HS^- (M)	8.64E-06	n.m.	7.48E-08	n.m.	n.m.	1.8E-05	b.d.l	n.m.	n.m.	8.11E-07	n.m.	n.a.	n.a.	1.5E-07
NO_3^- (M)	8.12E-06	n.m.	9.52E-07	n.m.	n.m.	1.08E-07	7.16E-07	n.m.	n.m.	1.47E-06	n.m.	6.29E-08	6.27E-05	9.68E-07
NH_4^+ (M)	b.d.l.	n.m.	3.88E-06	n.m.	n.m.	2.22E-06	1.33E-05	n.m.	n.m.	1.94E-06	n.m.	1.39E-06	b.d.l.	b.d.l.
Na^+ (M)	1.24E-01	n.m.	2.51E-03	n.m.	n.m.	3.39E-03	1.45E-02	n.m.	n.m.	2.15E-03	n.m.	1.13E-03	6.43E-02	4.51E-02
K^+ (M)	1.18E-03	n.m.	3.47E-05	n.m.	n.m.	4.20E-05	1.23E-04	n.m.	n.m.	5.58E-05	n.m.	4.69E-05	5.50E-04	4.02E-04
Mg^{2+} (M)	7.68E-05	n.m.	4.14E-05	n.m.	n.m.	3.43E-05	2.06E-07	n.m.	n.m.	3.97E-04	n.m.	7.67E-04	2.06E-05	9.87E-05
Ca^{2+} (M)	2.86E-02	n.m.	2.69E-04	n.m.	n.m.	5.18E-04	2.37E-03	n.m.	n.m.	4.99E-04	n.m.	1.15E-03	1.74E-03	1.89E-03
Fe^{2+} (M)	8.95E-06	n.m.	b.d.l.	n.m.	n.m.	b.d.l.	b.d.l.	n.m.	n.m.	<8.95E-07	n.m.	0.00E+00	b.d.l.	2.69E-06
Fe^{3+} (M)	8.95E-06	n.m.	2.69E-06	n.m.	n.m.	1.07E-05	b.d.l.	n.m.	n.m.	<8.95E-07	n.m.	7.16E-06	b.d.l.	2.69E-06
Ba^{2+} (M)	3.22E-6	n.m.	5.68E-7	n.m.	n.m.	5.1E-7	1.17E-6	n.m.	n.m.	5.02E-7	n.m.	4.51E-7	5.46E-6	6.63E-6
TDS(mg/L)	10,122	n.m.	204	n.m.	n.m.	296	n.m.	n.m.	n.m.	188	n.m.	256	3809	2971

Table A.2. Comparison between noble gas-derived residence times and ^{14}C ages for fracture waters in previous studies, and calculated oxygen isotope exchange equilibrium time for samples.

Sample Name	Temperature (°C)	pH	Residence Time (Ma)		14C Age (kyr)[£]	Oxygen isotope equilibrium time at pH = 7 (kyr)	Oxygen isotope equilibrium at pH = 9 (kyr)
			Closed system	Open system			
KL445	55	8.0	(21-105)[†]	(2.7-15.6)[†]		2.9	12.9
TT107	51	8.6	0.77-6.1[*]	0.1-1.0[*]	1.41–5.68	3.4	14.7
TT109	48	8.5			16.3–21.9	3.8	16.3
TT118	51	6.5				3.4	14.7
MP99	45	8.6	(15.8-25.0)[§]			4.3	18.0
MP120	65	8.2				1.9	9.3
DR5IPC	27	7.4	2.6-12.0[*]	0.2-0.69[*]	16.4–22.9	9.4	33.7
DR9IPC	24	8.8				10.7	37.6
JO129	40	9.0				5.3	21.3
MM546	41	7.7	40-97[*]	3.4-10.8[*]		5.1	20.6

[†] Data from Lippmann et al. (2003), based on a sample collected from a borehole located on a level above sample form this study.
[*] Data from Heard et al. (2018), based on samples from the same boreholes as samples from this study.
[§] Data from Lin et al. (2006), based on a sample collected from a borehole located between the MM99 and MM120 samples from this study.
[£] Data from Simkus et al. (2016).

Table A.3. Estimation of sulfate productivity by IROP and accumulated sulfate concentrations over 1-100 Ma in fracture waters in the Witwatersrand Basin, South Africa.

Lithology	Porosity* (%)	U* (ppm)	Th* (ppm)	K* (%)	S‡ (%)	Sulfate productivity (M/yr)	$[SO_4^{2-}]$ accumulated over 1 Ma (M)	$[SO_4^{2-}]$ accumulated over 100 Ma (M)
Carbon leaders	0.1	40,000	8,000	1	0.02	8.8E-10	8.8E-4	8.8E-2
					1.3	5.7E-8	0.057	5.7
Transvaal dolomite	5	0.6	5	0.56	0.02	2.8E-15	2.8E-9	2.8E-7
					1.3	1.8E-13	1.8E-7	1.8E-5
Ventersdorp	2	0.83	5.2	1.45	0.02	1.5E-14	1.5E-8	1.5E-6
					1.3	9.5E-13	9.5E-7	9.5E-5
Upper Witwatersrand	1	2.33	10.9	1.91	0.02	4.4E-14	4.4E-8	4.4E-6
					1.3	2.9E-12	2.9E-6	2.9E-4
Lower Witwatersrand	0.5	1.3	7.3	1.47	0.02	6.4E-14	6.4E-8	6.4E-6
					1.3	4.2E-12	4.2E-6	4.2E-4
Upper Vredefort	0.25	2.43	12.65	3.57	0.02	3.0E-13	3.0E-7	3.0E-5
					1.3	1.9E-11	1.9E-5	1.9E-3
Lower Vredefort	0.12	0.4	7.05	3.43	0.02	5.2E-13	5.2E-7	5.2E-5
					1.3	3.4E-11	3.4E-5	3.4E-3

* data from Lin et al. (2005a, b).
‡ data from Guy (2012).

Table A.4. Comparison between measured sulfate concentration and accumulated sulfate concentration by IROP over the residence time of fracture waters in the Witwatersrand Basin, South Africa.

Sample sites	**Residence time (Ma)**	**Host rock**	**IROP sulfate productivity (M/yr)**	**IROP accumulated [SO_4^{2-}] (M)**	**Measured [SO_4^{2-}] (M)**
Driefontein	0.2 to 12 Ma	Transvaal dolomite	2.8E-15 to 1.8E-13	5.6E-10 to 2.2E-6	1.38E-4 to 6.4E-4
Kloof	2.7 to 105 Ma	Ventersdorp Supergroup	1.5E-14 to 9.5E-13	4.1E-8 to 1.0E-4	9.85E-5
Mponeng	3.4 to 97 Ma			5.1E-8 to 9.2 E-5	4.94E-4
Tau Tona	16 to 25 Ma	Witwatersrand Supergroup	4.4E-14 to 4.2E-12	7.0E-7 to 1.1E-4	1.03E-4 to 1.17E-3
Joel	no data				3.67E-4
Masimong	40-97 Ma			1.8E-6 to 4.1E-4	7.03E-6